An accelerated lambda iteration method for multilevel radiative transfer

III. Noncoherent electron scattering

G.B. Rybicki[1] and D.G. Hummer[2,3]

[1] Harvard-Smithsonian Center for Astrophysics, 60 Garden Street, Cambridge, MA 02138 USA
[2] Max-Planck-Institut für Astrophysik, Postfach 1523, D-85740 Garching, Germany
[3] Institut für Astronomie and Astrophysik der Universität München, Scheinerstr. 1, D-81679 München, Germany

Abstract.
Since the mass of the electron is very small relative to atomic masses, Thomson scattering of low-energy photons ($h\nu \ll m_e c^2$) produces thermal Doppler frequency shifts that are much larger than atomic Doppler widths. A method is developed here to evaluate the electron scattering emissivity from a given radiation field which is considerably faster than previous methods based on straightforward evaluation of the scattering integral. This procedure is implemented in our multilevel radiative code (MALI), which now takes full account of the effects of noncoherent electron scattering on level populations, as well as on the emergent spectrum. Calculations using model atmospheres of hot, low-gravity stars display not only the expected broad wings of strong emission lines but also effects arising from the scattering of photons across continuum edges. In extreme cases this leads to significant shifts of the ionization equilibrium of helium.

Key words: radiative transfer – noncoherent Thomson scattering – non-LTE – stellar atmospheres

1. Introduction

The scattering by electrons of low-energy photons ($h\nu \ll m_e c^2$) is important in astrophysical situations only under the rather special circumstance that the electron-scattering opacity is not too much smaller than that from all other sources. Thomson scattering in these cases has traditionally been regarded as coherent in frequency, and much work on spectrum formation has been based on this assumption. However, if the spectrum of the object in questions contains features with a width less than or comparable to the electron Doppler width, such as strong lines and continuum edges, the scattering may have to be treated as noncoherent, i.e. the change in the frequency of the scattered photon by the electron Doppler effect must be taken into account (Münch 1948, Hummer & Mihalas 1967, Auer & Mihalas 1968a, 1968b). Although the description of this redistribution process as a convolution of the mean intensity $J(\nu)$ with a redistribution function is simple in principle, its inclusion

in numerical calculations leads to considerable difficulties in practice for three reasons. 1) The scale of the redistribution in frequency is much larger than the atomic Doppler line widths; 2) the evaluation of the convolution at each frequency involves an integration over a wide band of surrounding frequencies; 3) this coupling of frequencies conflicts with the basic strategy of approximate lambda iteration (ALI) methods which involve a frequency-by-frequency evaluation of the approximate lambda operator.

The transfer equation for two level systems accounting for noncoherent electron scattering have been solved in various approximation by a number of workers. Early work on this problem was based on the formulation in terms of a "reversing layer" by Chandrasekar (1948), who found a solution for the case in which the reddening of scattered photons arising from the Compton effect was included. Subsequently Münch (1948) considered the effects of electron Doppler redistribution, again in terms of a "reversing-layer" model, by means of a Fourier transform in frequency. This and other early work is summarized in Chapter 12 of Chandrasekhar (1960). Numerical solutions have been given for lines in the atmospheres of O-type stars by Auer and Mihalas (1968a, 1968b),who assumed complete redistribution for the atomic scattering. Rangarajan et al (1991) give solutions for parameterized models with both both partial and complete redistribution in the line.

Hillier (1991) and Hamann et al. (1992) have included noncoherent electron scattering (NES) in computing the emergent line spectra of realistic models of Wolf-Rayet stars, for which the effects are clearly observable. However, in these works NES is included only during the formal solution for the emergent spectra, after the level populations have been fixed from an NLTE solution in which NES has not been taken into account.

In this paper we develop a numerical method for the solution to radiative transfer problems in which noncoherent electron scattering can play an important role. The method is based on approximating the electron scattering redistribution function by a sum of exponentials. It is shown that only two exponential terms give a very accurate approximation. The electron scattering emissivity as a function of frequency at each point in the atmosphere then can be expressed through the solution to two simple differential equations in frequency space.

The corresponding difference equations can be solved numerically by Gaussian elimination. This procedure is easily included in any iterative solution of the combined radiative transfer and statistical equilibrium equations.

In previous schemes for evaluating the NES emissivity, the computing time for each depth in the atmosphere scales as $N_F N_W$, where N_F is the number of frequency grid points, and N_W is the number of frequency grid points needed to represent adequately the width of the electron redistribution function. For applications to spectral lines with structure on scales of both atomic and electron Doppler widths, N_W can be of order of 10–50 or larger. The present method scales more favorably as $C N_F$, where C is a small constant, independent of the frequency grid. It also automatically enforces exact conservation of photon number.

In this paper we describe an implementation of our method of treating noncoherent electron scattering for the multilevel ALI code MALI (Rybicki & Hummer, 1991, 1992; hereafter RHI, RHII). In contrast to previous methods (Hillier 1991, Hamann et al. 1992), full account is taken of the effect of NES on the level populations, as well as on the emergent spectrum. Although the particular application described here is to MALI, the method presented here is quite general and should be easily adaptable to other codes as well, especially ALI codes.

It should be made clear that in this latest generalization of MALI noncoherent electron scattering is treated not fully by ALI, but only by means of *ordinary* lambda iteration. This was not by choice, but resulted from a failure to find suitable approximate electron scattering operators to use in an ALI method. In particular, we tried several approximate operators based on coherent scattering, which is already solved non-iteratively in MALI. All of our choices were either unstable or had very poor convergence properties.

Fortunately, for many cases of interest, the mean number of photons scatterings due to electron scattering is very moderate, of order a few tens. Since the typical number of iterations in an ALI solution can be of order many tens to a hundred, the treatment of NES by ordinary lambda iteration in these cases will not substantially change the net number of iterations required for a solution. One should also note that numerical accelerators, such as Ng's (1974) method, used in MALI, act to improve the convergence of ordinary lambda iteration, as well as ALI. However, for problems with mean numbers of scatterings of order of a hundred or more, the present method is simply not suitable, and other methods will have to be developed.

In Sect. 2 we present the basic description of the electron redistribution problem. In Sect. 3 we develop the approximate exponential fit to the electron scattering redistribution function and show how the emissivity can be found by solving two differential equations. We then give results illustrating the accuracy of our approximation and the basic features of two-level transfer problems including electron scattering treated as coherent and incoherent processes. Sect. 4 describes the incorporation of our method into MALI and gives results for a hot O-star atmosphere including noncoherent electron scattering. As expected, the effects on individual lines were quite noticeable, as were the effects within a few electron Doppler widths of continua. However, we also found an unexpected and potentially important effect for certain continua, which, in the absence of noncoherent scattering, are strongly in absorption. Then scattering of radiation from the stronger continuum below the edge into the other can cause a substantial anomalous ionization of material, and conseqently a substantial change in the radiation field across the entire ionizing continuum, not just in the neighborhood of the jump.

2. Basic equations

The angle-averaged emissivity at frequency ν for unpolarized electron scattering in the non-relativistic limit can be written $j(\nu) = \sigma_T E(\nu)$, where σ_T is the Thomson cross section and $E(\nu)$ is the scattering integral,

$$E(\nu) \equiv \int_0^\infty R(\nu, \nu') J(\nu')\, d\nu'. \tag{1}$$

Here $J(\nu)$ is the mean intensity, and $R(\nu, \nu')$ is the unpolarized, angle-averaged electron scattering redistribution function. This relation holds at each spatial point in the medium; however, we shall suppresss this spatial dependence in the notation. The *noncoherent* scattering expressed by Eq. (1) is to be distinguished from *coherent* scattering, for which $E(\nu) = J(\nu)$.

Hummer & Mihalas (1967) derived explicit forms for the redistribution functions for non-relativistic electron scattering assuming negligible Compton energy shift. It is convenient for our purposes to express their results in terms of a modified function $\tilde{R}(y)$,

$$R(\nu, \nu') = \frac{1}{\beta_T \nu'} \tilde{R}(y), \tag{2}$$

where the variable y is defined by

$$y = \frac{\ln \nu - \ln \nu'}{\beta_T} = \frac{1}{\beta_T} \ln \frac{\nu}{\nu'}. \tag{3}$$

The quantity β_T is the mean electron thermal speed divided by the speed of light c,

$$\beta_T = \frac{1}{c}\sqrt{\frac{2kT}{m_e}} = 1.84 \times 10^{-5}\, T^{1/2}, \tag{4}$$

where T is the temperature in Kelvin, m_e is the electron mass, and k is Boltzmann's constant.

Hummer & Mihalas (1967) gave two forms for $\tilde{R}$, depending on whether isotropic scattering or the more exact dipole scattering is assumed; these are usually distinguished by the subscripts A and B, respectively. Their results are[1]:

$$\tilde{R}_A(y) = \ \mathrm{ierfc}\,\frac{|y|}{2} = \frac{1}{\sqrt{\pi}} e^{-y^2/4} - \frac{|y|}{2}\,\mathrm{erfc}\,\frac{|y|}{2}, \tag{5}$$

$$\tilde{R}_B(y) = \frac{3}{2}\,\mathrm{ierfc}\,\frac{|y|}{2} - 12\,\mathrm{i}^3\mathrm{erfc}\,\frac{|y|}{2} + 96\,\mathrm{i}^5\mathrm{erfc}\,\frac{|y|}{2}$$
$$= (\frac{11}{10} + \frac{2}{5}y^2 + \frac{1}{20}y^4)\frac{1}{\sqrt{\pi}}e^{-y^2/4}$$
$$- (\frac{3}{2} + \frac{1}{2}y^2 + \frac{1}{20}y^4)\frac{|y|}{2}\,\mathrm{erfc}\,\frac{|y|}{2}. \tag{6}$$

The functions $\mathrm{i}^n\mathrm{erfc}$ denote repeated integrals of the error function, defined, e.g., in Abramowitz & Stegun (1964; Sect. 7.2). These have been expressed in terms of the ordinary error function erfc by means of recurrence relations.

---

[1]The occurrences of "erf" in the formulas of Hummer & Mihalas (1967) are typographical errors, which should be replaced by "erfc".

Formulas (5) and (5), when substituted into Eq. (2), give redistribution functions that differ from those given by Hummer & Mihalas (1967), in that the "line center" frequency ν_0 does not appear, and the variable y is now defined in terms of logarithms of the frequencies ν and ν'. These changes have been made so that the resulting formulas apply for the whole spectrum, not just to a region in the neighborhood of a single line. It is appropriate in the non-relativistic limit that the redistribution process should depend primarily on the *ratio* of frequencies rather than the *differences* that appear in the Hummer and Mihalas formulas. This dependence on frequency ratio comes about because the Compton energy shift is negligible in the non-relativistic limit and the energy shift of a photon in the scattering process is due solely to the Doppler shifts into and out of the rest frame of the electron. (see, e.g., Rybicki & Lightman 1979; Sect. 7.3).

It can easily be verified that formulas (5) and (5) lead to the Hummer & Mihalas forms when applied to line transfer for cases of interest in stellar atmospheres, where $\beta_T \ll 1$, implying that the redistribution functions are sharply peaked near $\nu \approx \nu'$. An appropriate expansion of y is then

$$y \approx \frac{\nu - \nu'}{\beta_T \nu_0}, \tag{7}$$

where ν_0 can be taken to be either ν or ν', or, as in Hummer & Mihalas (1967), the line center frequency ν_0. Likewise, the overall factor in Eq. (2) can be replaced by $1/(\beta_T \nu_0)$.

However, for the present work the full logarithmic definition (3) for y will be used. In fact, it is convenient to introduce the logarithmic frequency variable

$$\xi = \log \nu, \tag{8}$$

which will be used instead of the frequency ν. Making the change of variables in Eqs. (1) and (2), we obtain

$$E(\xi) = \beta_T^{-1} \int_{-\infty}^{\infty} \tilde{R}(\beta_T^{-1} |\xi - \xi'|) J(\xi') \, d\xi', \tag{9}$$

where $E(\xi)$ and $J(\xi)$ now denote the scattering integral and mean intensity as functions of the variable ξ.

Since photon numbers are conserved upon scattering, the following integrals should be equal

$$\int_0^{\infty} \frac{E(\nu) \, d\nu}{h\nu} = \int_0^{\infty} \frac{J(\nu) \, d\nu}{h\nu}. \tag{10}$$

(The intensities here are defined in terms of energy, so one must divide by $h\nu$ to convert to photon numbers.) In terms of the logarithmic variable ξ, this relation may be written,

$$\int_{-\infty}^{\infty} E(\xi) \, d\xi = \int_{-\infty}^{\infty} J(\xi) \, d\xi. \tag{11}$$

Substituting Eq. (9) and demanding that the resulting equation hold for all functions $J(\xi)$, we find the normalization condition

$$\int_{-\infty}^{\infty} \tilde{R}(y) \, dy = 1, \tag{12}$$

which is exactly satisfied for both forms (5) and (5).

This normalization condition (12) also justifies the use of coherent scattering as an approximation when the scale of variation of the radiation field is large compared to the electron Doppler width. In that case, $J(\xi')$ can be taken from under the integration in Eq. (9), replacing ξ' by ξ, and the normalization condition implies the coherent result $E(\xi) = J(\xi)$. Coherent scattering is usually a good approximation for continua, but it can fail badly in the neighborhood of lines and continuum edges, as we shall see.

Another quantity of importance is the second moment

$$\int_{-\infty}^{\infty} \tilde{R}(y) y^2 \, dy = \frac{1}{2}, \tag{13}$$

which measures the effective width of the redistribution function. This moment has the same value $(1/2)$ for both forms (5) and (5). The second moment is particularly important for describing noncoherent electron scattering in cases where large numbers of scatterings occur, such as in the far wings of lines. In this case, the frequency behavior can be well described by a random walk that depends solely on the two moments (12) and (13).

By contrast, the fine details in the centers of lines depend primarily on the absolute value of the function $\tilde{R}(y)$ near $y = 0$. For this reason the value of $\tilde{R}(0)$ is very important, and also, to a lesser extent, its (right) derivative $\tilde{R}'(0^+)$. These quantities differ for the isotropic and dipole cases, and are given by,

$$\tilde{R}_A(0) = \frac{1}{\sqrt{\pi}}, \qquad \tilde{R}_A'(0^+) = -\frac{1}{2}, \tag{14}$$

$$\tilde{R}_B(0) = \frac{11}{10\sqrt{\pi}}, \qquad \tilde{R}_B'(0^+) = -\frac{3}{4}. \tag{15}$$

3. The exponential approximation

An efficient method for the evaluation of the integral in Eq. (9) can be based on a simple approximation to the modified redistribution functions $\tilde{R}(y)$ in the form of a sum of N exponential terms:

$$\tilde{R}(y) = \frac{1}{2} \sum_{i=1}^{N} a_i b_i \exp(-b_i |y|). \tag{16}$$

We shall call this the *exponential approximation*, but it should be noted that, in terms of true frequencies, the approximation actually takes the *power law* form,

$$\tilde{R}(y) = \frac{1}{2} \sum_{i=1}^{N} a_i b_i \left(\frac{\nu_<}{\nu_>} \right)^{b_i/\beta_T}, \tag{17}$$

where $\nu_<$ and $\nu_>$ are, respectively, the smaller and larger of ν and ν'.

3.1. Fitting procedures

Sets of constants a_i and b_i can be determined in a number of ways, all of which depend on matching some properties of the approximate and true functions. In view of the importance of conditions (12) and (13), we demand that coefficients should accurately satisfy the relations

$$\sum_{i=1}^{N} a_i = 1, \tag{18}$$

$$\sum_{i=1}^{N} a_i b_i^{-2} = \frac{1}{2}. \tag{19}$$

The simplest exponential approximation consists of one term ($N = 1$), with two independent coefficients a_1 and b_1 chosen to satisfy both Eqs. (18) and (19), namely, $a_1 = 1$ and $b_1 = \sqrt{2}$. Since Eqs. (18) and (19) are the same for both isotropic and dipole forms for $\tilde{R}(y)$, this approximation does not distinguish between them.

Improved approximations can be obtained by using two terms ($N = 2$), with four independent coefficients, giving two additional degrees of freedom as compared with the single term approximation. In view of the importance of the behavior of $\tilde{R}(y)$ near $y = 0$, we would like to use these new degrees of freedom to fit the value and slope of the redistribution function at the origin, given by Eq. (14) or (15). These conditions require that the following two equations be satisfied,

$$\sum_{i=1}^{N} a_i b_i = 2\tilde{R}(0), \tag{20}$$

$$\sum_{i=1}^{N} a_i b_i^2 = -2\tilde{R}'(0^+), \tag{21}$$

Note that the four conditions expressed by Eqs. (18) through (21) are all of the same general form,

$$\sum_{i=1}^{N} a_i b_i^m = S_m, \tag{22}$$

with different values of m. Approximations for larger N constructed by fitting higher order moments and higher order derivatives will also satisfy equations of this form.

Equation (22) represents a set of nonlinear equations for the unknown values of the coefficients a_i and b_i. In general, numerical methods must be used to solve them[2]. We used the Newton-Raphson iterative method and confined our search to real solutions; complex solutions imply oscillating exponential terms that give unacceptable negative values for $\tilde{R}(y)$ for large y.

We attempted to solve the above $N = 2$ system of equations for the isotropic and dipole functions. However, these nonlinear equations apparently do not have (real) solutions when both the value and slope are given their exact values. Thus we chose to fit the value exactly and to fit the slope as closely as possible, namely, -0.333 (instead of -0.5) for the isotropic case and -0.6 (instead of -0.75) for the dipole case. The results obtained in this way are summarized in Table 1.

In Fig. 1 the exact functions $\tilde{R}$ for isotropic and dipole case are plotted along with the corresponding exponential approximations. The maximum relative errors over the range

---

[2]In the special case where the values of m are equally spaced, equations of the form (22) can be solved analytically by Prony's method (see, e.g., Hildebrand 1974). However, Prony's method often produces complex solutions.
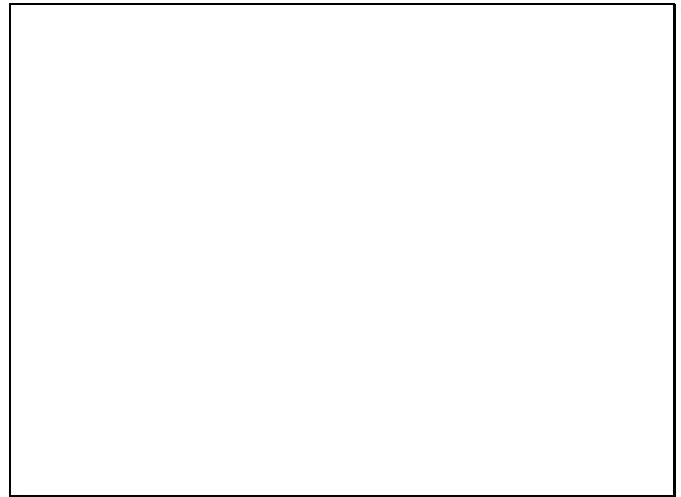
Fig. 1. Exact and approximate redistribution functions $\tilde{R}(y)$ for a) isotropic and b) dipole

Table 1. Coefficients for exponential approximation

Type	N	i	a_i	b_i
A1&B1	1	1	1.000000000000	1.414213562373
A2	2	1	5.682790496584	1.835757192503
		2	-4.682790496584	1.986816272751
B2	2	1	1.690703717290	1.614249968779
		2	-0.690703717290	2.154326524957

$0 \leq y \leq 3$ for the $N = 1$ approximations are about 25% for the isotropic and about 17% for the dipole. The maximum relative errors for $N = 2$ approximations over this range are both about 10%. For values beyond $y = 3$ the relative error of the approximation increases rapidly, since the true redistribution function decays asymptotically faster than exponential. However, at $y = 3$ the absolute values of these functions have already decreased by about two orders of magnitude from their values at $y = 0$, so the region $y > 3$ should not be a substantial source of error in the emissivities.

There is reason to expect solutions based on these approximations to be more accurate than the above maximum errors might suggest. Note that these approximations have been specifically constructed to be exact for the values and moments of the redistribution functions that are most critical for the solution. Also, the treatment of electron scattering involves integration over the redistribution function and this tends to average out the errors.

3.2. Reduction to differential equations

One of the advantages of the exponential representation is that the evaluation of the scattering integral E can be reduced to the solution of differential equations. To see this, let us substitute Eq. (16) into Eq. (9), leading to

$$E(\xi) = \sum_{i=1}^{N} a_i F^{(i)}(\xi), \tag{23}$$

where

$$F^{(i)}(\xi) = \frac{1}{2} b_i \beta_T^{-1} \int_{-\infty}^{\infty} \exp(-b_i \beta_T^{-1} |\xi - \xi'|) J(\xi') \, d\xi'. \qquad (24)$$

Differentiating twice with respect to ξ, one easily shows that $F^{(i)}(\xi)$ satisfies the second-order differential equation

$$-\frac{\beta_T^2}{b_i^2} \frac{d^2 F^{(i)}(\xi)}{d\xi^2} + F^{(i)}(\xi) = J(\xi). \qquad (25)$$

One property of this differential approximation is that it exactly preserves the normalization condition (11). To show this, we integrate Eq. (25) over ξ, which gives

$$\int_{-\infty}^{\infty} F^{(i)}(\xi) \, d\xi = \int_{-\infty}^{\infty} J(\xi) \, d\xi, \qquad (26)$$

assuming that the first derivative of $F^{(i)}$ vanishes at both endpoints of the region of integration. This will generally be true if the frequency range is chosen so that the radiation field is sufficiently small at the limits of the range, or by explicit choice of boundary conditions (see Appendix A). Now multiplying by a_i and summing over all i, using Eqs. (18) and (23), the normalization condition (11) is recovered.

The radiation transfer problem can be treated numerically by introducing a frequency grid ξ_j, $j = 1, \ldots, P$. All functions of frequency are then represented by the set of their values on this grid, e.g., $E_j = E(\xi_j)$. Eq. (23) then gives the values of electron scattering emissivity on the grid,

$$E_j = \sum_{i=1}^{N} a_i F_j^{(i)}, \qquad (27)$$

in terms of the quantities $F_j^{(i)} = F^{(i)}(\xi_j)$. These quantities can be determined by solving the differential equation (25) for each value of i by means of the well known Feautrier method. The details of the numerical method are given in Appendix A. A proof that the numerical method also preserves the correct normalization (11) is given in Appendix B.

3.3. Relation to the Kompaneets equation

The differential equation method of the last section bears some superficial similarity with the treatment of electron scattering using the Kompaneets equation (Kompaneets 1957; Rybicki and Lightman 1979, Sect. 7.6), which is closely related to the Fokker-Planck equation. However, as we now explain, the two methods are very different in their range of validity and in their mathematical structure.

The major advantage of the Kompaneets equation is that it includes the major physical effects associated with electron scattering: 1) the frequency spreading due to the thermal Doppler effect; 2) the frequency shift due to thermal Doppler effect (inverse Compton effect); 3) the frequency shift due to electron recoil (Compton effect); and 4) stimulated electron scattering. Because of this, it is applicable to many aspects of Comptonization phenomena. Its major limitation is that it can only describe radiation fields that vary slowly on the scale of the frequency shift per scattering. In particular, the Kompaneets equation is not appropriate for treating the neighborhoods of lines or continuum edges.

The differential equation method of this paper treats only the first physical effect above, namely, the thermal Doppler spreading effect. However, its major advantage is that it can treat radiation fields that vary rapidly on the scale of typical frequency shifts. This is essential for treating lines and continuum edges in typical stellar atmospheres, where, fortunately, the other physical effects treated by the Kompaneets equation are usually not very important.

The mathematical distinction between the two methods is very striking. Let us compare the Kompaneets equation with the $N = 1$ approximation of this paper, where $E(\xi) = F^{(1)}(\xi)$. Then both methods are formulated using second-order differential operators. However, the Kompaneets equation expresses the *emissivity* as a differential operator acting on the *radiation field*; in contrast, the differential equation (25) expresses the *radiation field* as a differential operator acting on the *emissivity*. Thus, our second-order operator is not directly comparable to the Kompaneets operator but rather to its *inverse*. It is this distinction that allows our method to treat rapidly varying radiation fields.

A further mathematical point is that our method can be improved by going to larger values of N, with no noticeable numerical problems. An analogous improvement of the Kompaneets equation would involve the introduction of higher order differential operators; however, it is known that this can lead to numerical problems, such as instabilities and negative solutions.

3.4. Tests of the method

In order to test the exponential approximation method, it was applied to some simple, parametrized models. A specially written, non-iterative numerical code was developed for this purpose, so that the results could be evaluated directly, without being confused by questions of iterative convergence. We shall present one particular such parametrized model here; another will be presented in Sect. 4.2.
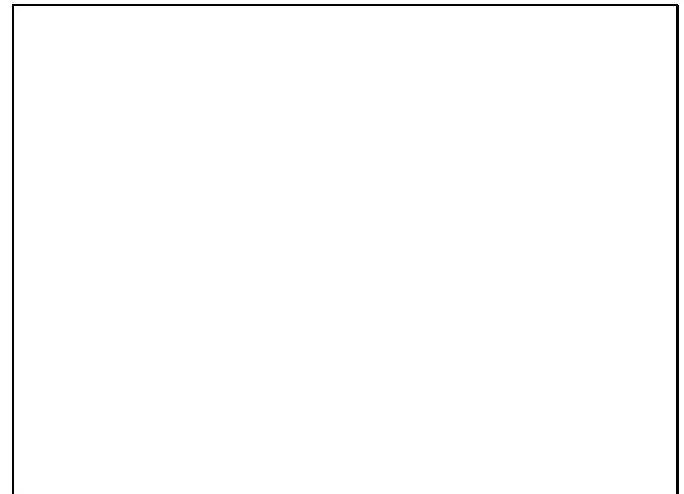
Fig. 2. $\log F_x$ (arbitrary units) vs. x for parametrized model using coherent and various noncoherent scattering approximations

In Fig. 2 is shown one result of applying the non-iterative code. The case is one of pure line scattering in a finite slab of total line mean optical depth $\tau_L = 2 \times 10^4$ and total electron

scattering optical depth $\tau_e = 20$. The photon injection rate into the line is uniform with depth. The log of the emergent flux F_x (in arbitrary units) is plotted against x, the frequency relative to line center in units of the line Doppler width. The mass of the ion is assumed to be that of hydrogen, so that the electron Doppler width is ~ 43 in these units. This is an extreme case for which line photons are scattered many times ($\sim \tau_e^2$) by the electrons, leading to wide wings extending out to many line Doppler widths. The two parts of this figure examine the flux over very different frequency bands: Fig. 2a shows the details near the center of the line, $|x| < 20$, while Fig. 2b shows the behavior in the far electron-scattering wings, $|x| < 1000$.

Four types of curves are plotted in Fig. 2. The curves marked C give the result assuming that the electron scattering is coherent. The remaining curves are marked according to the type of redistribution function assumed, A for isotropic and B for dipole, and also by the number of terms in the exponential approximation.

One sees immediately that the coherent solution is vastly different from the other three solutions, which are themselves very similar. The behavior for large x shown in Fig. 2b is particularly striking, in that all the noncoherent solutions are graphically indistinguishable in the electron-scattering wings; this is explained simply as the result of all three approximations having the correct zeroth and second moments of the redistribution function. The only place where distinctions between the three noncoherent cases can be seen is just outside the line core, where the differences between the values of $\tilde{R}(0)$ are important.

The overwhelming impression from Fig. 2 is that the differences in the solutions due to different forms of the noncoherent approximation are far less important than the differences with the coherent approximation. We conclude that any of the various noncoherent approximations will do acceptably well. From a theoretical point of view we prefer the dipole form, since it is physically more realistic than the isotropic one. Therefore, all further numerical calculations reported in this paper will use the $N = 2$ dipole approximation (B2).

4. Implementation in MALI

The form of the approximate lambda iteration method developed in RHI and RHII is implemented in the FORTRAN program MALI. Since the publication of RHII the code has been generalized to treat line overlaps and an arbitrary number of chemical species.

Although the implementation described here is specific for MALI, it should be easily adaptable to other numerical codes, especially to ALI codes.

4.1. Electron scattering by lambda iteration

The evaluation of the electron-scattering emissivity described in Sect. 3 has been implemented in MALI to treat noncoherent electron scattering by lambda iteration, while all bound-bound and bound-free processes continue to be treated with our ALI procedure.

The frequency grid is constructed with double points at every continuum edge to allow for discontuities in the radiation field. On both sides of every edge and line up to twenty additional frequency points are included with a spacing of a specified fraction of the electron scattering Doppler width at some fiducial temperature. A mapping is constructed to and from

a secondary frequency grid without double points, on which the difference Eqs. (A1) with boundary conditions (A3) are to be integrated, and the factors weighting J_j^- and J_j^+ in Eq. (A4) are stored. In each iteration, after J_ν is evaluated, the difference equations are solved at every depth point using the modified Feautrier procedure given in Appendix I of RHI and the electron-scattering emissivity is evaluated from Eq. (27).

The electron-scattering emissivity and opacity are taken together with those of the free-processes as forming the "background opacity and emissivity" χ_c and η_c which appear in Eqs. (2.6) and (2.7) of RHII. These are then updated after every iteration, i.e. are treated by lambda iteration. The cost of this operation per iteration scales as the product of the numbers of depth and frequency points, i.e. in the same way as integration of the monochromatic transfer equations. In practice the additional time required for the calculation of the electron-scattering emissivity is hardly discernable. However, the additional frequency points needed to resolve spectral features on the order of the electron-scattering Doppler width do lead to moderate increases in the computation time.

For coherent electron scattering by lambda iteration one simply sets $E_j = J_j$. In RHII, coherent electron scattering was treated by direct integration of the monochromatic transfer equation in vector form. For a variety of test cases the results for coherent scattering calculated from the direct solution and by lambda iteration were found to be identical, thus confirming the validity of lambda iteration for electron scattering while all other processes are included in the ALI procedure. However, for the realistic model atmospheres discussed below, the convergence from LTE initial populations is very slow, and the iterations are started from populations calculated by the direct method. The iterative solutions for coherent scattering then converges to exactly the same results as the direct solution.

4.2. Discussion of results
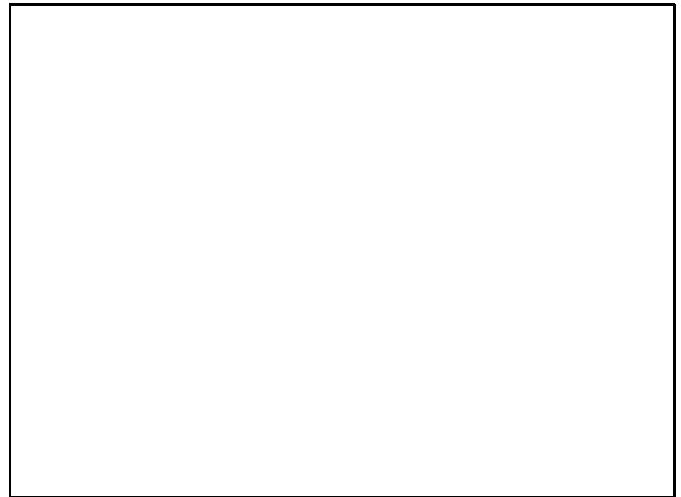
Fig. 3. Electron density and temperature as functions of mass column density for Model 2

To illustrate the type of effects produced by noncoherent electron scattering, we have input into MALI photospheric temperature and density structures from non-LTE models for early O-type stars, computed by Dietmar Kunze. These models con-

tain only hydrogen and helium; the relative abundances, effective temperatures and surface gravities are given in Table 2. The model at $T_{\text{eff}} = 50000\,\text{K}$ is represented in Fig. 3; the other two are qualitatively similiar.

Table 2. Model atmosphere parameters

Model	T_{eff}	$\log g$	$N(\text{He})/N(\text{H})$
1	40000 K	4.00	0.100
2	50000 K	3.74	0.100
3	60000 K	4.20	0.111

In our calculations the temperature and total atom density as a function of the mass column density were specified and held fixed. The original run of electron density was used only to calculate the initial LTE populations, and subsequently the electron density was calcuated from the ion populations after every iteration. The converged electron density was found to be essentially identical to that of the original model, as were the level populations deep in the atmosphere where the diffusion approximation is valid. As distinct from the original models, the results obtained here for noncoherent scattering will not be in strict radiative equilibrium because of the changes in atomic level population.

We employed simplified atomic models: H^0 with five bound levels, He^0 with 17 and He^+ with three. Doppler line profiles, which were used in the calculation of the atmospheric structure, are also assumed here. This is not realistic for the calculation of the surface flux, but permits the comparison of coherent and noncoherent scattering without introducing further complications, and should not influence our conclusions.
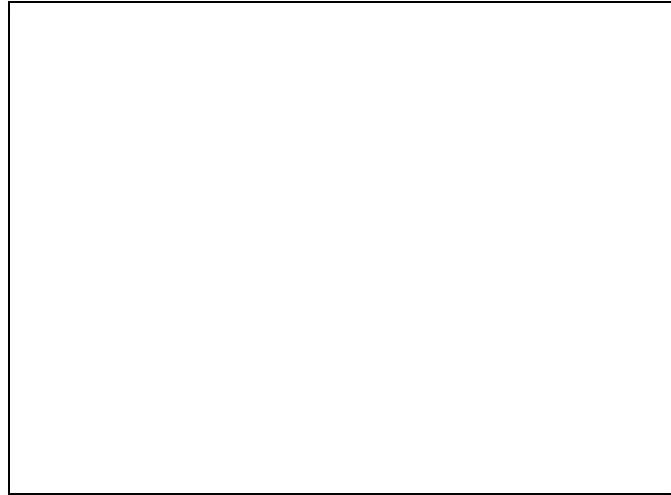

Fig. 4. Surface flux versus frequency for Model 2 computed with coherent (dotted) and noncoherent (solid) scattering

We concentrate now on Model 2, which with $T_{\text{eff}} = 50000\,\text{K}$ and $\log g = 3.74$ lies close to the Eddington limit. The surface flux is shown in Fig. 4. The largest differences between the results for coherent and noncoherent electron scattering are found in the regions around the He II edge, the H I edge and Lyman α, which are expanded in Figs. 5, 6, and 7, respectively.


Fig. 5. Detail from Fig. 4 of the He II continuum
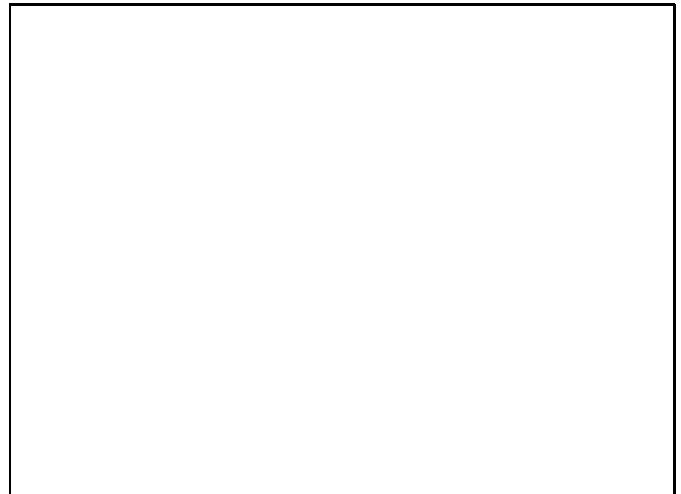
Fig. 6. Detail from Fig. 4 of the H I continuum
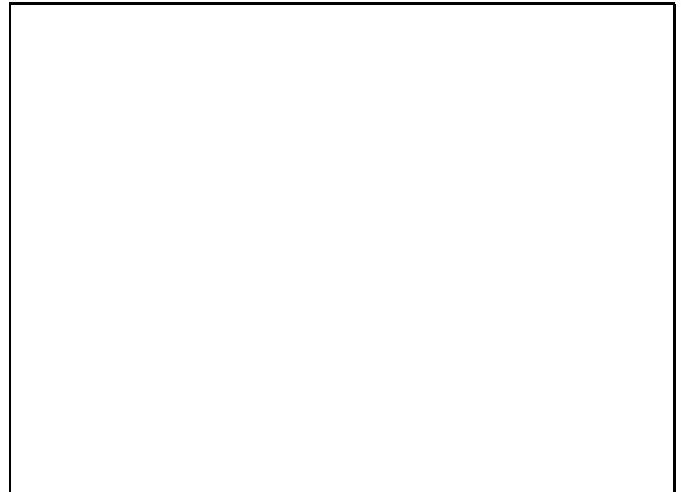
Fig. 7. Detail from Fig. 4 of the Lyman α line
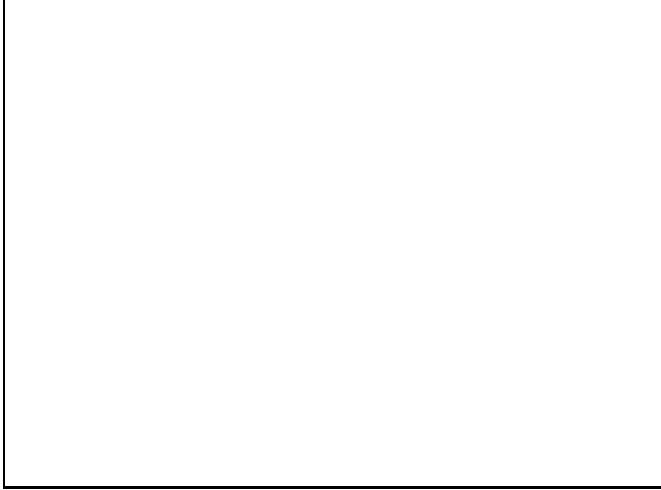
Fig. 8. Ionization fractions as functions of mass column density for Model 2 computed with coherent (dotted) and noncoherent (solid) scattering

The gas is essentially completely ionized; the ionization fractions H^0/H, He^0/He and He^+/He are given in Fig. 8. In Figs. 4–8 dotted and solid lines represent coherent and noncoherent scattering, respectively.

Most conspicuous in Figs. 4 and 5 are the order of magnitude increase in the flux in the He II continuum and the decrease in the flux just below the edge caused by the noncoherent electron scattering. These effects arise from the scattering by electrons of the intense radiation just below the edge into the threshold region where the photoionization cross section has its maximum. This increases the ionization rate of He^+ by an order of magnitude, and thus shifts the ionization balance of He^0 by the same amount. The resulting decrease in the populations of He^0 and He^+ are clearly seen in Fig. 8. Note that the additional flux in the He II continuum arises not just from the photons scattering across the edge, but rather from those escaping from the atmosphere because the the He^+ population is reduced.

The behavior at the H I edge, shown in Fig. 6, is completely different. Now the only effect of noncoherent electron scattering is appearance of the "spur" just below the edge. This feature is caused by scattering of radiation from the Lyman continuum, which throughout much of the atmosphere is strongly in emission, to the region just below the threshold. This occurs even in models for which the surface flux in the Lyman continuum is in absorption. As no additional radiation is fed into the threshold region of the Lyman continuum, and the amount lost is very small, the ionization balance is not significantly affected.

The narrow emission wings of Lyman α shown in Fig. 7 for coherent electron scattering are examples of the Schuster effect. Non-coherence reduces this effect by scattering the radiation into the very long wings. The slight deepening of the absorption feature arises because the radiation trapped in the line core is scatterd out into the wings. However, this effect is weak and in other cases the core is slightly shallower with non-coherence.

The general behavior of some of the other spectral lines can be summarized as follows. The Lyman β line is similiar in appearance to Lyman α but less deep. The three He I resonance lines and He II Lyman α are entirely in absorption with broad, very shallow wings. Balmer α is weakly in absorption, as are most of the He subordinate lines, although a few line of He I are weakly in emission with long shallow wings. All emission and absorption lines are weaker for noncoherent than for coherent electron scattering.

The above effects are found to a reduced extent in the model with $T_{\rm eff} = 60000\,{\rm K}$, $\log g = 4.2$, and are present only weakly in the model with $T_{\rm eff} = 40000\,{\rm K}$, $\log g = 4.0$. The ionization equilibrium in the surface layers shifts by roughly factors of 3.5 and 1.7, respectively. This shows that the decisive feature is the essentially complete ionization of the gas, so that the weak electron-scattering opacity is not completely overshadowed.

It might also be objected that these phenomena will be radically reduced by the lines converging on the series limit. Equating the electron Doppler width to the ionization potential of a hydrogenic ion shows that the corresponding principal quantum number is approximately

$$n^* = 23.3\,T_4^{-1/4}, \tag{28}$$

where $T_4 = T/(10^4\,{\rm K})$. States with n down to at least this value will be involved in shifting of photons in or out of the continuum. Thus, two or three electron Doppler widths at the temperatures considered here corresponds to a state below the region of confluence. In other words, radiation present below the line merging region will continue to cause additional ionization.

4.3. Effect of metal absorption

The inclusion of metals is likely to reduce both the enhanced He II emission and the H I spur. However, for hot, low-gravity stars near the Eddington limit, absorption by *bound-free* transitions of metal ions should not substantially reduce the shift of the ionization balance, as species with appreciable abundances have ground state ionization edges lying in the He II continuum, and thus will themselves become more highly ionized, just as He itself.

The effect of metal lines, on the other hand, is not easy to determine *a priori*. The dense array of metal lines (arising mostly from Fe IV and Fe V) between the H I and He II continua illustrated in Fig. 14c of Pauldrach et al (1994) for a *plane parallel* stellar model with $T_{\rm eff} = 50500\,{\rm K}$ and $\log g = 3.785$ suggests that metal lines could reduce or quench entirely the additional ionization of He. More appropriate would be *spherical* models including wind effects – the so-called unified models (Gabler et al (1992) and references therein). These give fluxes in the He II continuum larger than thoses in corresponding plane parallel models by some orders of magnitude, which would shift the ionization equilibria of the metals to higher stages (the ionization potential of Fe IV is only 0.4 eV larger than that of He II). Moreover, deep in atmosphere of a hot star, the line blocking shifts to higher frequencies, while the scattering of radiation into the He II continuum persists. The combined effects of these mechanisms remains to be investigated.

The main effects found here arise from the flow of radiation from deep hot parts of the atmosphere in relatively transparent parts of the spectrum, followed by scattering by electrons into the opaque regions, such as ionizing continuum and strong lines. Such effects are not, of course, limited to stellar photospheres. Winds of hot stars could be affected, as the scattering

of radiation in continuua would allow ions to receive ionizing radiation from the photosphere which would otherwise be cut off by the increasing red-shift of the stellar radiation as seen by the material in the wind. Clouds illuminated by an external source of ionizing radiation could also experience an increase in the degree of ionization by the same mechanism. Whether or not these possibilities are realized in any particular case must be investigated. The technique developed here should make that possible.

A. Appendix: The numerical method

Applying the second-order Feautrier method to Eq. (25), we obtain,

$$-\frac{\beta_T^2}{b_i^2}\left[\frac{F_{j-1}^{(i)}}{\Delta_{j-1/2}\Delta_j} - \frac{2F_j^{(i)}}{\Delta_{j-1/2}\Delta_{j+1/2}} + \frac{F_{j+1}^{(i)}}{\Delta_{j+1/2}\Delta_j}\right]$$
$$+F_j^{(i)} = J_j, \quad (A1)$$

for $j = 2, \ldots, (P-1)$, where,

$$\Delta_{j-1/2} = \xi_j - \xi_{j-1}, \qquad \Delta_{j+1/2} = \xi_{j+1} - \xi_j,$$
$$\Delta_j = \frac{1}{2}(\xi_{j+1} - \xi_{j-1}). \quad (A2)$$

Equation (A1) gives $(P-2)$ recurrence relations for the P unknowns $F_j^{(i)}$. In order to solve these equations, they must be supplemented by appropriate boundary conditions at the ends of the grid. A particularly convenient set of boundary conditions are those of zero derivative, which ensure the proper normalization condition (see Eq. [26] and the discussion following it). The zero derivative conditions can be expressed to second-order accuracy using the method of Auer (1967), which gives,

$$\left(\frac{2\beta_T^2}{b_i^2\Delta_{3/2}^2} + 1\right)F_1^{(i)} - \frac{2\beta_T^2}{b_i^2\Delta_{3/2}^2}F_2^{(i)} = J_1$$
$$-\frac{2\beta_T^2}{b_i^2\Delta_{P-1/2}^2}F_{P-1}^{(i)} + \left(\frac{2\beta_T^2}{b_i^2\Delta_{P-1/2}^2} + 1\right)F_P^{(i)} = J_P \quad (A3)$$

When applying these difference equations, a problem arises at a continuum discontinuity, where the radiation field J has a separate left and right limit. In order to represent the radiation field near such a discontinuity we assign two values for J_j, namely, J_j^- for the left limit and J_j^+ for the right. In this case, the value J_j in Eq. (A1) may be replaced with the quantity

$$\tilde{J}_j = \frac{\Delta_{j-1/2}J_j^- + \Delta_{j+1/2}J_j^+}{\Delta_{j-1/2} + \Delta_{j+1/2}}, \quad (A4)$$

that is, with an appropriately weighted average of the left and right limits of J at the jth point. It can be shown that

this procedure is equivalent to assigning separate frequency points for the left and right limits and then letting these two points approach each other (the proof of this statement will be omitted here).

Equations (A1) and (A3) constitute a tridiagonal system of equations for the values of $F_j^{(i)}$ on the grid, which can be solved, as usual, by the method of Gaussian elimination. This is done for each value of i (i.e., two values for the $N=2$ exponential approximations), and the results summed according to Eq. (27) to give the desired values of E_j. The operations count for this solution scales linearly with the number of frequencies P. Furthermore, the coefficient of P is quite small, since only simple algebraic operations are involved. This compares very favorably with other methods of applying a convolution operator to a very unevenly spaced grid.

The preceding method for computing the emissivity must be done separately for each spatial point (depth) in the medium. The coefficients of the difference equations (A1) and (A3) depend on depth, but solely through the temperature dependence of β_T, so a good deal of pretabulation of coefficients is possible. The computation time necessary to find the emissivity at all depths and frequencies scales simply as the number of frequency points times the number of depth points. Typically these emissivity computations will represent only a moderate fraction of the total time needed for the solution of the entire radiative transfer problem.

B. Appendix: Normalization of the method

Using the discrete equations of Appendix A, it can be shown that normalization condition (11) holds exactly, providing the integrals there are appropriately interpreted in terms of the trapezoidal rule. The derivation of this result will include the possibility of discontinuities in J, as given in Eq. (A4). Starting with Eq. (A1) (with $\tilde{J}_j$ replacing J_j), we multiply by Δ_j to obtain,

$$\frac{1}{2}F_j^{(i)}\Delta_{j-1/2} + \frac{1}{2}F_j^{(i)}\Delta_{j+1/2} = \quad \frac{1}{2}J_j^-\Delta_{j-1/2} + \frac{1}{2}J_j^+\Delta_{j+1/2}$$
$$+(G_{j+1/2}^{(i)} - G_{j-1/2}^{(i)}), \quad (B1)$$

where $G_{j+1/2}^{(i)} \equiv (\beta_T/b_i)^2(F_{j+1}^{(i)} - F_j^{(i)})/\Delta_{j+1/2}$. Likewise, Eqs. (A3) can be written,

$$\frac{1}{2}F_1^{(i)}\Delta_{3/2} = \frac{1}{2}F_1^{(i)}\Delta_{3/2} + G_{3/2}^{(i)}$$
$$\frac{1}{2}F_P^{(i)}\Delta_{P-1/2} = \frac{1}{2}F_P^{(i)}\Delta_{P-1/2} - G_{P-1/2}^{(i)}. \quad (B2)$$

Now summing Eqs. (B1) for $j = 2, \ldots, (P-1)$, and adding in both Eqs. (B2), we obtain

$$\sum_{j=2}^{P}\frac{1}{2}F_j^{(i)}\Delta_{j-1/2} + \sum_{j=1}^{P-1}\frac{1}{2}F_j^{(i)}\Delta_{j+1/2}$$
$$= \sum_{j=2}^{P}\frac{1}{2}J_j^-\Delta_{j-1/2} + \sum_{j=1}^{P-1}\frac{1}{2}J_j^+\Delta_{j+1/2}, \quad (B3)$$

Note that all of the $G^{(i)}$ terms have cancelled out. Rearranging summation indices, this can be written,

$$\sum_{j=1}^{P-1} \frac{1}{2}(F_j^{(i)} + F_{j+1}^{(i)})\Delta_{j+1/2} = \sum_{j=1}^{P-1} \frac{1}{2}(J_j^+ + J_{j+1}^-)\Delta_{j+1/2} \quad \text{(B4)}$$

Multiplying by a_i and summing over all i, using Eqs. (18) and (27), we obtain,

$$\sum_{j=1}^{P-1} \frac{1}{2}(E_j + E_{j+1})\Delta_{j+1/2} = \sum_{j=1}^{P-1} \frac{1}{2}(J_j^+ + J_{j+1}^-)\Delta_{j+1/2}. \quad \text{(B5)}$$

This result is the discrete version of the normalization condition (11), where the integrals have been evaluated using the trapezoidal rule over each segment of the grid.

References

Abramowitz M., Stegun I., 1964, Handbook of Mathematical Functions, U.S. Government Printing Office, Washington, D.C.

Auer L.H. 1967, ApJ 150, L53

Auer L.H., Mihalas D. 1968a, ApJ 153, 245

Auer L.H., Mihalas D. 1968b, ApJ 153, 923

Chandrasekhar S. 1948, Proc. R. Soc. London A192, 508

Chandrasekhar S. 1960, Radiative Transfer, Dover, New York

Gabler R., Gabler A., Kudritzki, R.P., Mendez, R.H. 1992, A&A 265, 656

Hamann W.-R., Leuenhagen U., Koesterke L., Wessolowski U., 1992, A&A 255, 200

Hildebrand F.B., 1974, Introduction to Numerical Analysis, 2nd ed., McGraw-Hill, New York

Hillier D.J. 1991, A&A 247, 455

Hummer D.G., Mihalas D., 1967, ApJ 150, L57

Hummer D.G., Rybicki G.B., 1992, ApJ 387, 248

Kompaneets, A.S., 1957, Sov. Phys. JETP 4,730

Mihalas D. 1978, Stellar Atmospheres, 2nd Ed., Freeman, San Francisco

Münch G. 1948, ApJ 108, 116

Ng, K.C., 1974, J. Chem. Phys. 61, 2680

Pauldrach A.W.A., Kudritzki R.P., Puls J., Butler K., Hunsinger J. 1994, A&A 283, 525

Rangarajan K.E., Mohan Rao D., Periah A. 1991, MNRAS 250, 633

Rybicki G.B., Hummer D.G., 1991, A&A 245, 171 (RHI)

Rybicki G.B., Hummer D.G., 1992, A&A 262, 209 (RHII)

Rybicki G.B., Lightman A.P., 1979, Radiative Processes in Astrophysics, John Wiley & Sons, New York

This figure "fig1-1.png" is available in "png" format from:

http://arXiv.org/ps/astro-ph/9404019v1
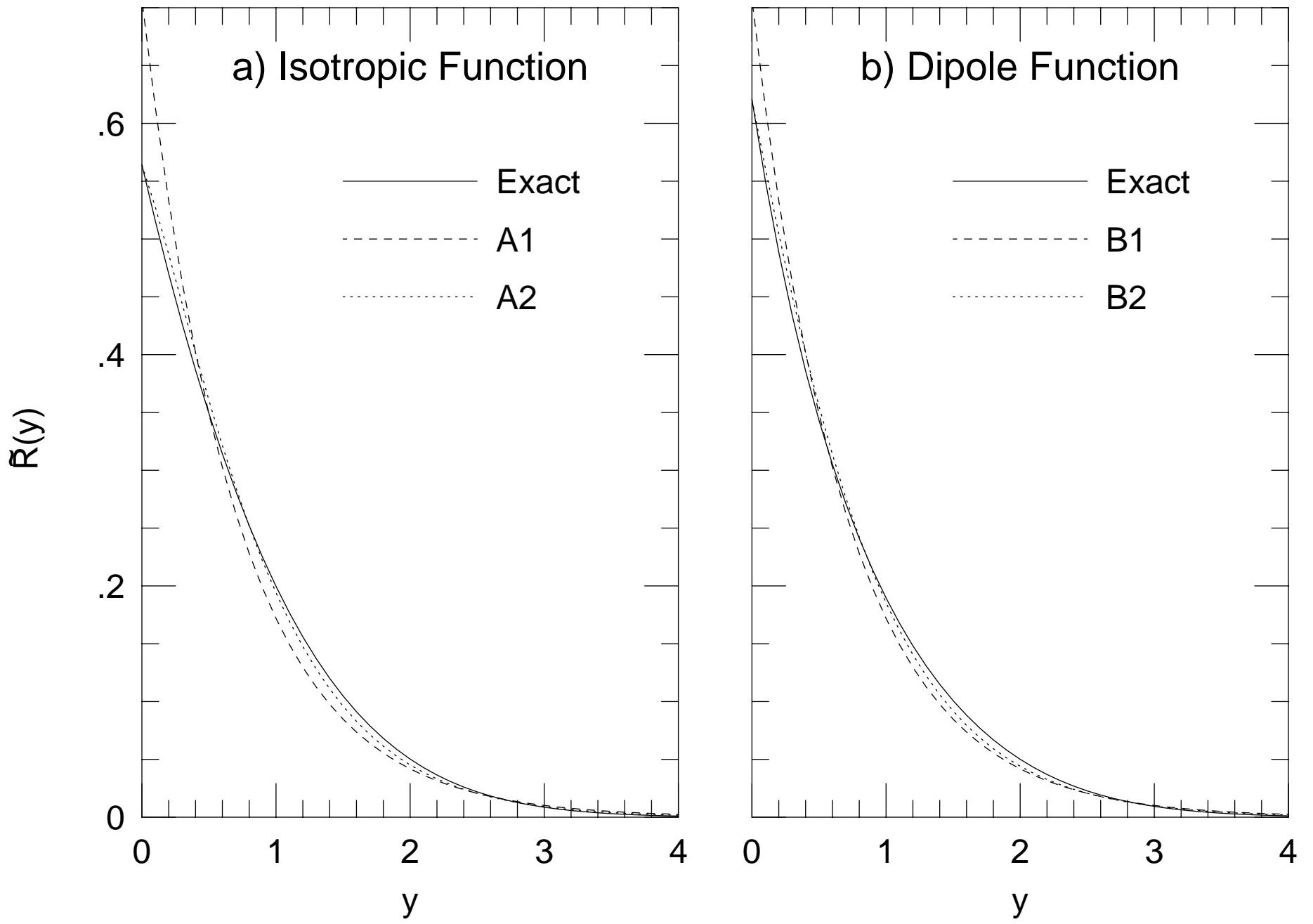
Figure 1

This figure "fig2-1.png" is available in "png" format from:

http://arXiv.org/ps/astro-ph/9404019v1

This figure "fig1-2.png" is available in "png" format from:

http://arXiv.org/ps/astro-ph/9404019v1

This figure "fig2-2.png" is available in "png" format from:

http://arXiv.org/ps/astro-ph/9404019v1
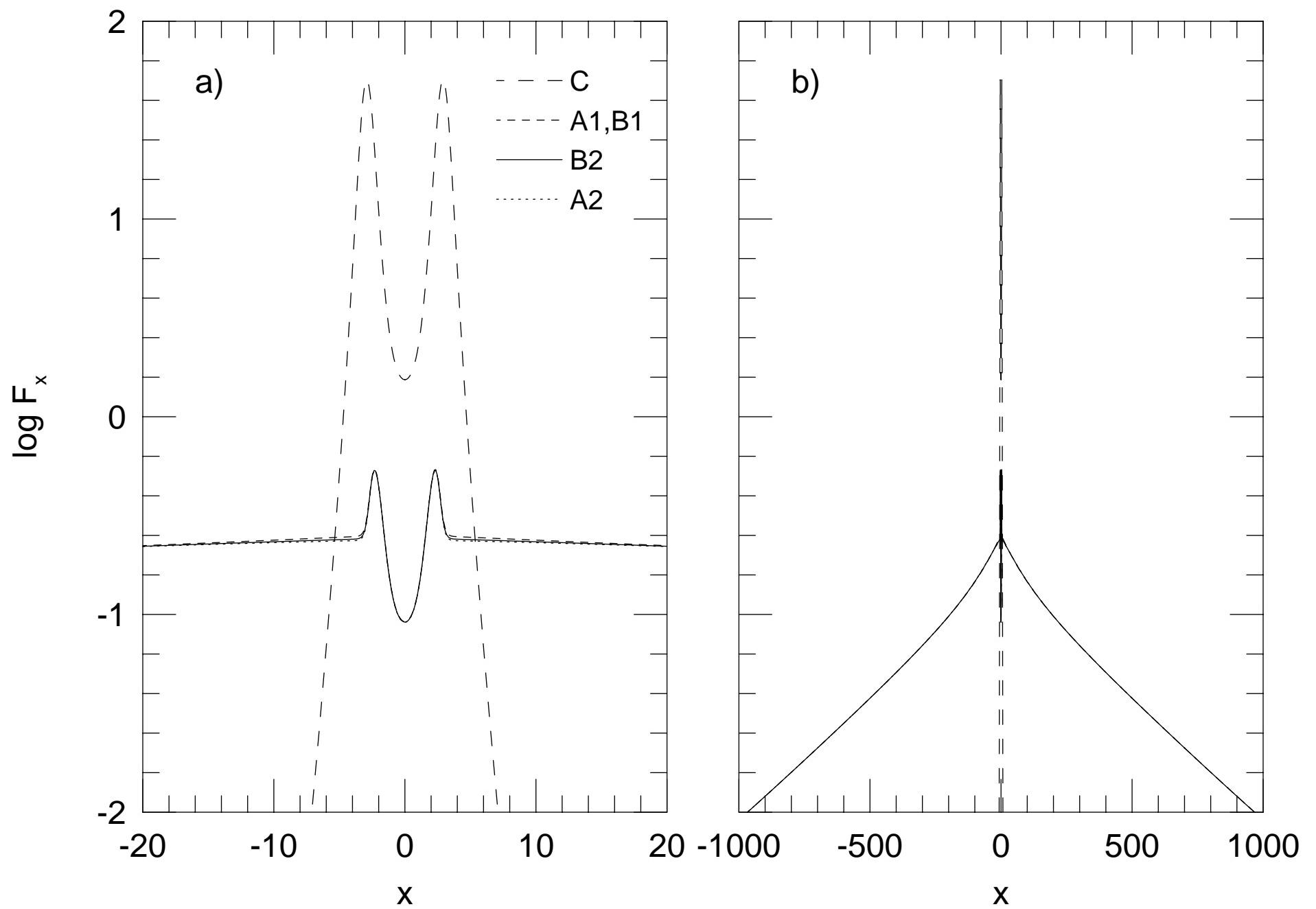
Figure 2

This figure "fig1-3.png" is available in "png" format from:

http://arXiv.org/ps/astro-ph/9404019v1

This figure "fig2-3.png" is available in "png" format from:

http://arXiv.org/ps/astro-ph/9404019v1
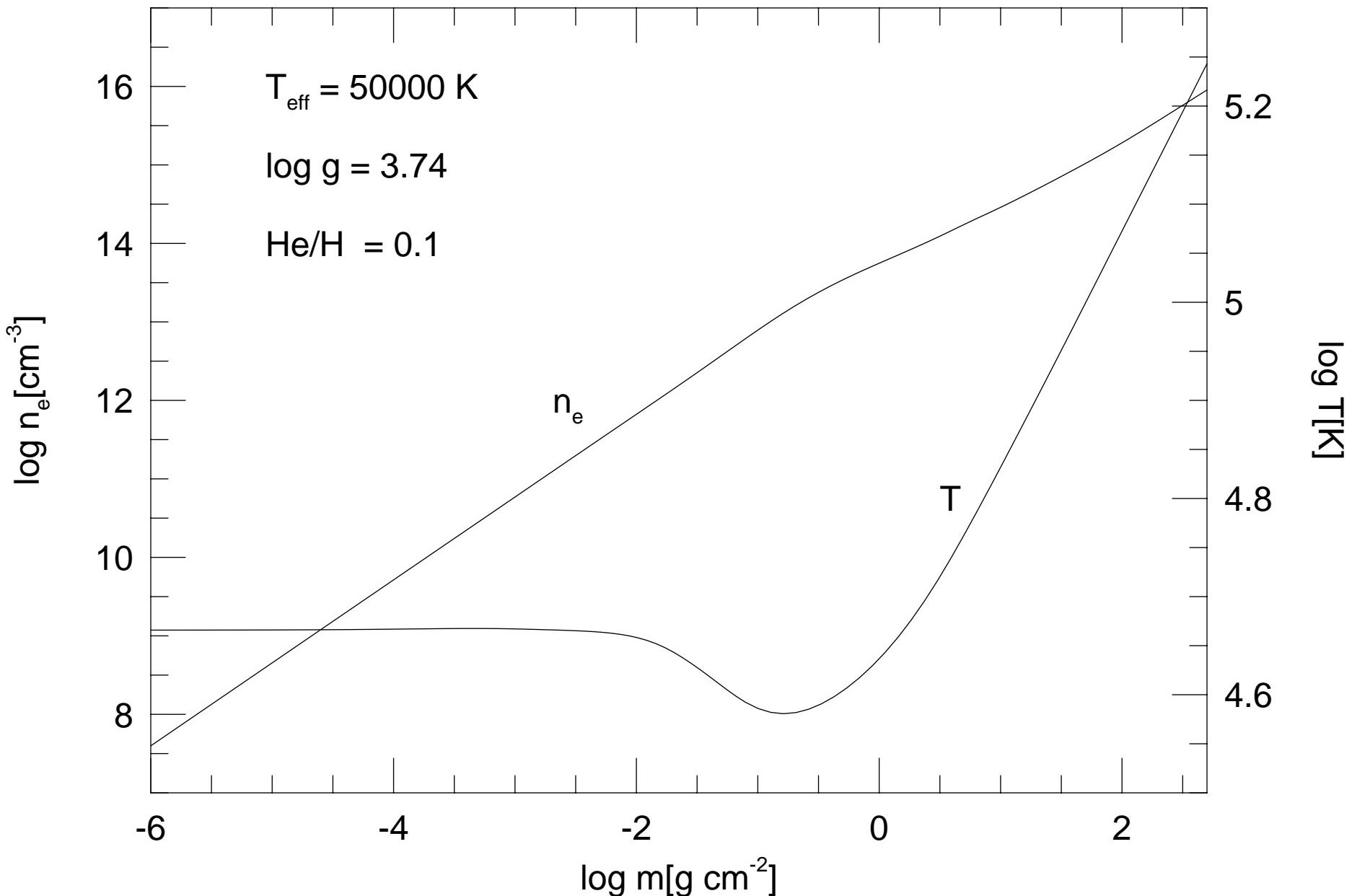
Figure 3

This figure "fig1-4.png" is available in "png" format from:

http://arXiv.org/ps/astro-ph/9404019v1
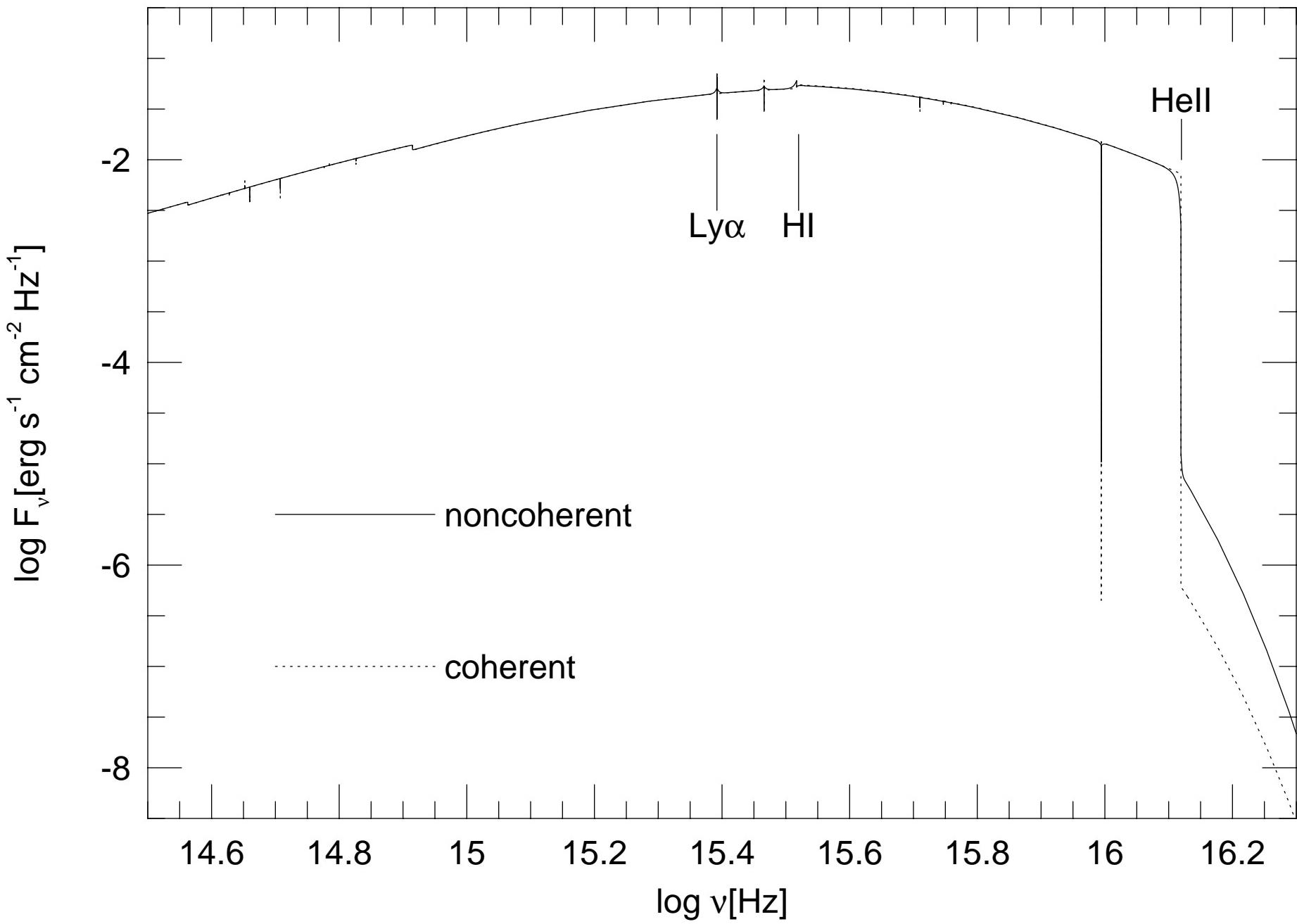
Figure 4

This figure "fig1-5.png" is available in "png" format from:

http://arXiv.org/ps/astro-ph/9404019v1
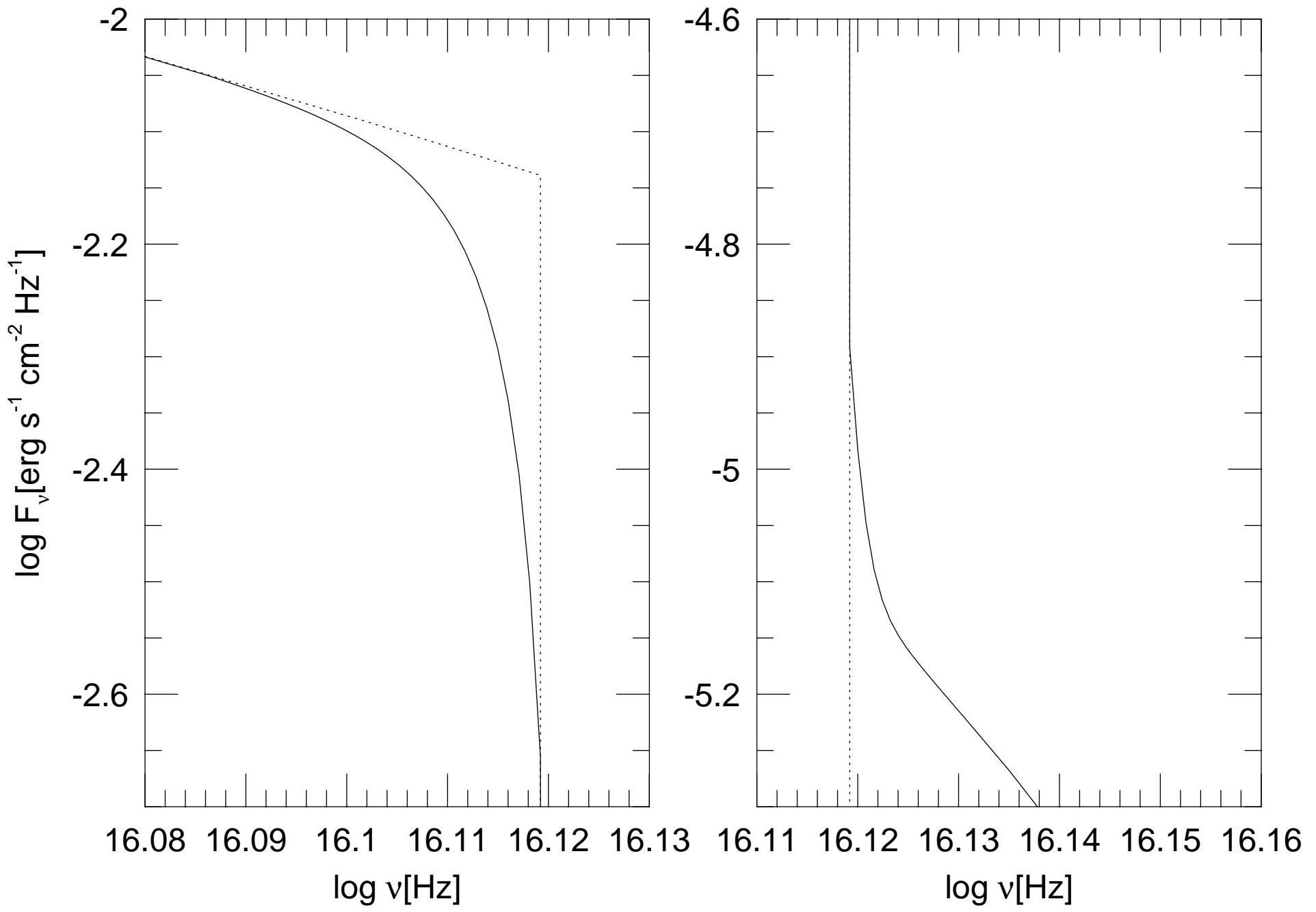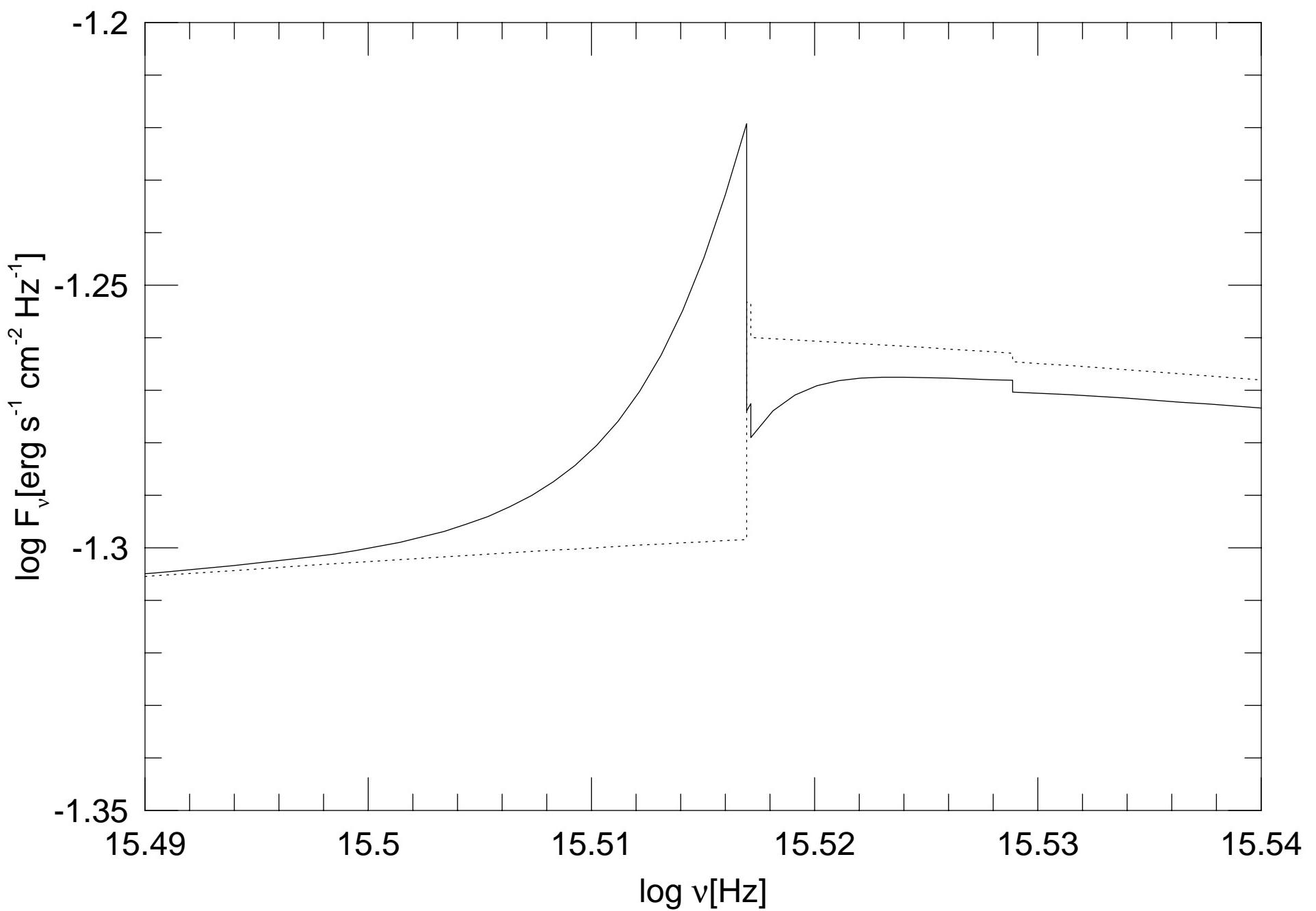
Figure 5

Figure 6

Figure 7

Figure 8